Ocean Data Assimilation, Initialization, and Predictions of ENSO with a Coupled GCM

EDWIN K. SCHNEIDER, BOHUA HUANG, ZHENGXIN ZHU, DAVID G. DEWITT, JAMES L. KINTER III, BEN P. KIRTMAN, AND J. SHUKLA

Center for Ocean–Land–Atmosphere Studies, Calverton, Maryland

(Manuscript received 9 February 1998, in final form 13 July 1998)

ABSTRACT

A scheme for making seasonal to interannual predictions of El Niño–Southern Oscillation with a coupled atmosphere–ocean general circulation model that incorporates subsurface ocean measurements in the initial conditions is described. Anomaly initial conditions are used in order to reduce initial shock and climate drift. The ocean component of the prediction model has a nearly global domain, and the coupled model does not employ anomaly coupling or empirical statistical corrections.

Initial conditions for the ocean were obtained from a near-global ocean analysis produced by an ocean data assimilation system. The assimilation system uses a variationally formulated optimal interpolation method to analyze oceanic fields from temperature observations and a first-guess field provided by integrating a global ocean general circulation model. The period of the analysis was 1986 through 1992.

The anomaly initial conditions for the ocean were generated by adding the anomalies of the assimilated fields from the assimilation climatology to the coupled model climatology. A series of 28 1-yr hindcast experiments, four each year for the years 1986–1992, was carried out to test the scheme. The hindcasts show considerable skill in the equatorial Pacific.

1. Introduction

Prediction of El Niño–Southern Oscillation (ENSO) variability, which is distinguished by large sea surface temperature (SST) anomalies in the eastern equatorial Pacific with a lifetime on the order of one year, is potentially important because these SST anomalies are associated with global-scale climatic consequences (Ropelewski and Halpert 1987). Stimulated by the pioneering work of Cane et al. (1986), a number of systems have been developed and tested for predicting ENSO variability. Latif et al. (1998) reviews those methods that have shown promise, including dynamical and statistical schemes of varying complexity. Hindcast experiments with the different systems have shown that the models have the potential to make useful forecasts for seasonal to interannual lead times. In forecast mode, these techniques have sometimes proved less successful than anticipated in predicting the occurrence and timing of warm, cold, or near-normal eastern Pacific SST; however, the number of events that have occurred during the verification period has not yet been large enough to produce reliable statistics. This paper reports on the development and application to hindcasts of a dynamical scheme that uses a coupled atmosphere–ocean general circulation model (GCM). The combination of features of this scheme that make it novel are that the GCM does not use flux correction, anomaly coupling, or other statistical corrections, that the ocean has a nearly global domain, and that initial conditions for the ocean are taken to be a combination of the coupled model's climatology and ocean state anomalies derived from a separate ocean data assimilation (ODA), which includes subsurface ocean data.

Dynamical schemes use coupled atmosphere–ocean models to predict ENSO variability from the local application of the laws of motion, analogous to the way that short- and medium-range dynamical weather forecasts are produced. In principle, a coupled atmosphere–ocean GCM is the most faithful approximation to the laws of motion in the hierarchy of dynamical models and should therefore produce the best forecast. However, practical difficulties prevent the coupled GCM approach from achieving its potential. The two most obvious problems are climate drift and initial shock.

Climate drift arises from errors in the dynamical model approximations to the physical laws and parameterizations of the physical processes. Because of these errors, the climate that the model approaches in a long integration generally has a different time-mean state as well as different higher-order moments than the actual climate. In dynamical system jargon, a model realization beginning from an initial condition off the model's cli-

Corresponding author address: Dr. Edwin K. Schneider, Center for Ocean–Land–Atmosphere Studies, 4041 Powder Mill Rd., Suite 302, Calverton, MD 20705-3106.
E-mail: schneider@cola.iges.org

mate attractor will approach and remain on the attractor during its evolution. This phenomenon is known as climate drift. Since the real climate system does not lie on the model attractor, a model forecast begun from observed initial conditions will contain systematic errors that grow in time until the model attractor is reached. Little is known about the manner in which the time-dependent systematic drift interacts with the anomalies that are being predicted. Climate drift is sometimes envisaged as a relaxation process proceeding most rapidly initially and slowing with time. However, in the equatorial waveguide, adjustment to unbalanced initial conditions occurs via eastward propagating Kelvin wave and westward propagating Rossby wave signals (e.g., McCreary 1978; Gill 1982, section 11.11). The direct Kelvin wave or reflected Rossby wave signal resulting from the initial imbalance will affect the SST and the future evolution of the coupled system on reaching the eastern Pacific. We will refer to this adjustment to unbalanced initial conditions as initial shock.

There is some evidence that coupled predictions depend sensitively on initial conditions (Ji and Leetmaa 1997), as expected in chaotic systems. If this is the case, it is important that the climate drift and especially the initial shock be eliminated for the predictions to be made successfully. On the other hand, Rosati et al. (1997) and Stockdale (1997) obtained skillful ENSO predictions in cases where the initial shock was not excluded, which would be the expected result if the coupled system were quasi-linear and nonchaotic.

One approach that is popular for eliminating climate drift is anomaly coupling (Ji et al. 1994; Kirtman et al. 1997). While the details of the procedures vary, in anomaly coupling, certain of the forcing fields are taken to be composed of an observed climatology plus anomalies (from the model climatology) as calculated by the model. For example, the wind stress as seen by the ocean is the observed annual cycle climatology plus the wind stress anomaly from the atmospheric model. This approach has the benefits of reducing climate drift and causing the coupled model climatology of the target fields (SST, wind stress, precipitation, sea level pressure) to be close to the observed. These benefits are obtained, however, by sacrificing the consistency of the model system with the underlying physical principles, such as conservation of energy and momentum, and continuity of fluxes.

In a preliminary investigation, hindcasts were made for 1987 (strong warm event) and 1988 (strong cold event) with a version of the coupled model, similar to the one described by Schneider et al. (1997), that used a low-resolution atmosphere without anomaly coupling. Ocean initial conditions were interpolated from an early version of the National Centers for Environmental Prediction (NCEP) ocean analysis (Ji et al. 1995). This procedure failed: the initial shock was manifested as a very strong warm event in both cases, with both approaching the same state after a few months. On the other hand, essentially the same model with anomaly coupling had been used successfully to hindcast these cases (Zhu and Schneider 1995). Our experience was then that some method for reducing the initial shock is important for good predictions.

We describe and evaluate a new prediction system here, which we refer to as the ''coupled system.'' The system consists of a coupled atmosphere–ocean GCM, in which the ocean domain is near global, and an ocean data assimilation (ODA) module. The coupled model does not employ anomaly coupling or statistical corrections at the atmosphere–ocean interface. The coupled GCM and the ODA both use the same ocean general circulation model (OGCM) configuration. The ocean initial conditions incorporate subsurface observations of ocean temperature and density as analyzed by the ODA. To avoid the problems of climate drift and the shock from insertion of observed data in the coupled model, anomaly initial conditions are used. That is, ocean initial conditions are obtained by adding the anomalies of the assimilated ocean from its climatology to the coupled model climatology. The atmospheric initial state is brought to near-equilibrium with the ocean initial conditions by a one-month spinup prior to coupling. This system has the benefits of using a physically consistent model and reducing climate drift and initial shock, but has the drawback of allowing large errors in the model climate.

The major new feature of our system is the use of anomaly initial conditions that incorporate subsurface ocean measurements. A variant of the anomaly initial conditions approach was used by Latif et al. (1993) but without subsurface data. The NCEP (Ji et al. 1996), Geophysical Fluid Dynamics Laboratory (GFDL; Rosati et al. 1997), and European Centre for Medium-Range Forecasts (ECMWF; Stockdale et al. 1998) systems employ assimilated subsurface ocean data in the initial conditions, but the NCEP system uses anomaly coupling to deal with the climate drift problem, while the GFDL and ECMWF systems do not attempt to remove climate drift except a posteriori.

A series of 28 12-month hindcasts was carried out using the coupled system, one hindcast every 3 months for the 1986–92 period of available analyses from the ODA. The results presented below show that the anomaly initial condition approach can potentially produce useful forecasts.

The sample size of 28 hindcasts is rather small. Also, the period for which the hindcasts was made is thought to be anomalously predictable (e.g., Ji et al. 1996). To address these concerns, estimates are given in appendix B of the statistical significance and representativeness of the results of the coupled system, using the much larger number of cases and years sampled from the anomaly coupled system.

The aim of this paper is to motivate and describe the implementation of the new scheme and to demonstrate that the further development of this scheme is warranted.

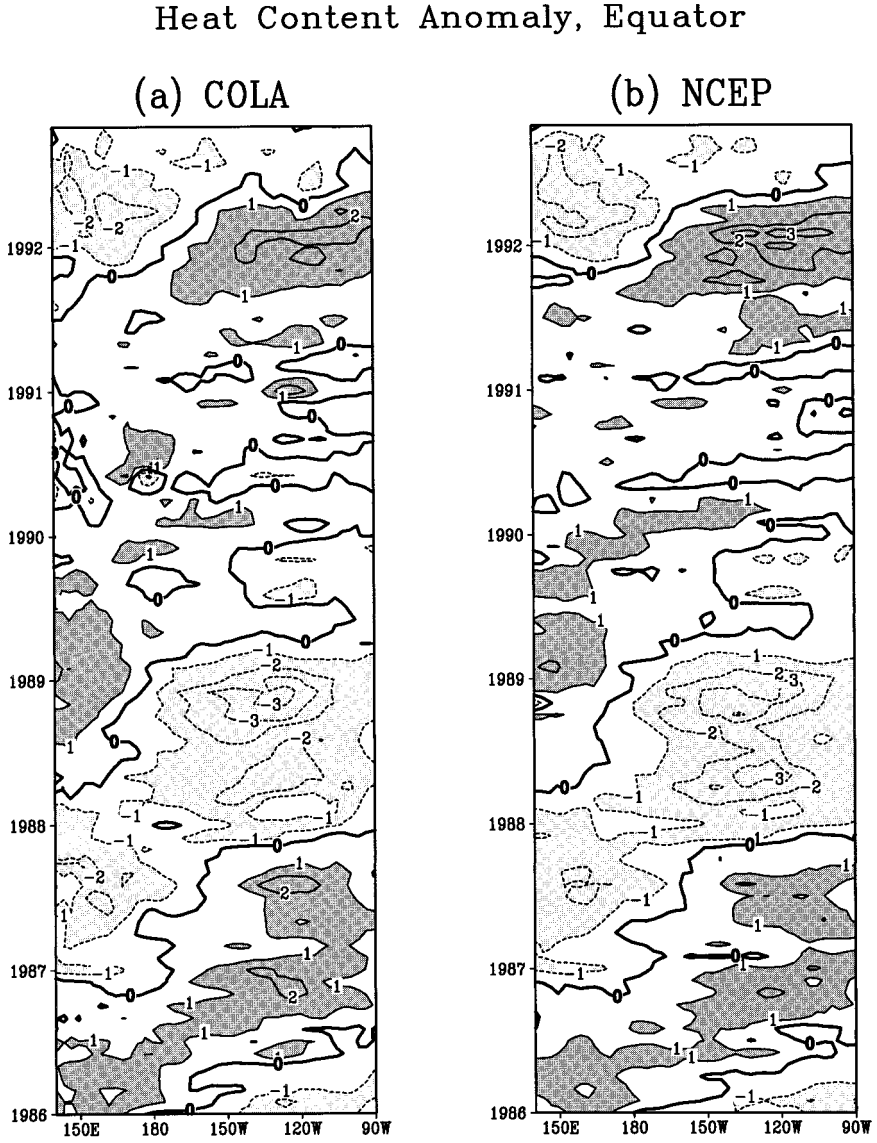

FIG. 1. Equatorial heat content anomalies from (a) COLA and (b) NCEP ocean data assimilation. Contour interval is 1°C. Areas with values greater than 1°C have dark shading, and areas with values less than −1°C have light shading.

It is not possible at this early stage of the research to suggest that the new scheme is superior to (or worse than) the other sophisticated statistical and dynamical ENSO predictions schemes that are in use.

2. Ocean data assimilation system

The evolution of the ocean between 70°S and 60°N during the period 1986–92 is approximated by the analysis of the ocean temperature and surface wind stress measurements interpolated in a dynamically consistent manner by variational optimal interpolation following Derber and Rosati (1989). Details of the COLA system are described in appendix A and in Huang and Kinter (1997).

The COLA assimilation produced monthly SST fields virtually indistinguishable from the U.S. Climate Prediction Center (CPC) analysis in the tropical ocean both for the mean field and for the annual and interannual variability. The heat content anomalies derived from the COLA analysis are also quite similar to those from the NCEP RA3 analysis (Ji and Smith 1995), as can be seen in Fig. 1. In the Pacific, the correlation between the heat content anomalies of the two analyses exceeds 0.8 everywhere between 10°S and 5°N. The correlation is less than 0.6 in the low-latitude Pacific only in a narrow

band near 10°N (see Fig. 9 of Huang and Kinter 1997). The effect of the assimilation of subsurface data on the heat content anomalies can be seen by comparing Figs. 1a and 9c of Kirtman and Schneider (1996). The latter figure displays the heat content anomalies obtained in an assimilation unconstrained by subsurface data. The most obvious differences are in the larger amplitude of the anomalies and the fine structure added by the assimilation of subsurface data.

3. Coupled model configuration and climatology

The coupled model combines the COLA atmospheric GCM (AGCM) and the GFDL Modular Ocean Model (MOM), version 1.0, ocean GCM. Brief descriptions of these models and the coupling procedure are given below. The integration that determined the coupled model climatology is described, and the model climatology and SST variability in the equatorial Pacific are compared with observations.

a. Atmospheric model

The atmospheric model is based on a global spectral model developed for medium-range weather forecasting (Sela 1980). A biophysically based land surface parameterization is included. The physical parameterizations of the atmosphere–land surface model used in these experiments are the same as those described by Schneider et al. (1997) with the following exceptions: the land surface model has been modified as described in Xue et al. (1996); the deep cumulus convection scheme is the relaxed Arakawa–Schubert scheme of Moorthi and Suarez (1992) as implemented by DeWitt (1996); and the diagnosed cloud fractions were modified as described below. The relaxed Arakawa–Schubert scheme was chosen to replace the moisture convergence closure deep convection scheme (a modification of Kuo 1965) used in previous coupled prediction experiments (Zhu and Schneider 1995; Kirtman et al. 1997) because of better simulation of the wind stress in the tropical Pacific in uncoupled AGCM simulations (Kirtman and DeWitt 1997).

The horizontal resolution of the atmospheric model is triangular truncation at total wavenumber 30 (T30). The vertical structure of the model is represented by 18 unevenly spaced levels using sigma (pressure normalized by surface pressure) as the vertical coordinate.

The cloud scheme was modified from the variant of the Slingo (1987) scheme documented by DeWitt (1996) in order to bring the atmospheric GCM into closer agreement with the top of the atmosphere radiative fluxes measured by satellite (DeWitt and Schneider 1997). The changes followed Kiehl et al. (1994) and led primarily to reduction in convective cloud fraction.

b. Ocean model

The ocean model is version 1 of the GFDL MOM (Bryan and Lewis 1979; Pacanowski et al. 1993), a finite-difference treatment of the primitive equations of motion using the Boussinesq and hydrostatic approximations in spherical coordinates, adapted as described in Schneider et al. (1997). The domain is that of the World Ocean between 70°S and 60°N. The coastline and bottom topography are realistic except that ocean depths less than 100 m are set to 100 m and the maximum depth is set to 4000 m. Major islands within the domain are treated realistically. The artificial high-latitude meridional boundaries are impermeable and insulating. The zonal resolution is 1.5°. The meridional grid spacing is 0.5° between 10°N and 10°S, gradually increasing to 1.5° at 20°N and 20°S and fixed at 1.5° in the extratropical oceans. There are 20 levels in the vertical with a constant layer depth of 15 m for the top 10 levels. The layer thicknesses for the bottom 10 levels are 15.2, 16.1, 20.0, 34.1, 75.9, 177.1, 375.9, 687.4, 1063.8, and 1384.5 m. Richardson number–dependent coefficients are chosen for the vertical mixing and diffusion of momentum, heat, and salinity (Pacanowski and Philander 1981). The horizontal viscosity and diffusivity coefficients are prescribed and set equal to a constant 2×10^7 cm^2 s^{-1}. A thermodynamic sea ice parameterization (Schneider and Zhu 1998, their appendix) is included, as the ocean model domain is nearly global.

Sunlight is attenuated exponentially with a 15-m *e*-folding depth in the ocean GCM in the coupled model. This parameterization is a potential source of error since it allows about 68% more sunlight to penetrate below the first model layer than is observed in clear water (Paulson and Simpson 1977), although the amount penetrating below the second layer is about the same as observed for clear water. The depth of the simulated mixed layer in the central and western tropical Pacific of a similar coupled GCM is sensitive to the details of this parameterization (Schneider and Zhu 1998).

c. Coupling

The atmosphere and ocean models are coupled once per day as described in Schneider et al. (1997), using the GFDL Modular Interface for Coupled Air–Sea Applications system (A. Rosati 1990, personal communication) to interpolate the coupling data between the atmospheric and ocean model grids. This coupling scheme is a preliminary version of the one incorporated in version 2 of MOM. The surface wind stress and heat flux supplied by the atmosphere to the ocean model are not modified in any way—no flux correction or anomaly coupling is used. In the region outside of the ocean domain, the SST is prescribed to be the climatological value of the Reynolds blended SST (Reynolds 1988) for that month. Monthly mean diagnostics were saved for analysis.

d. Coupled model climatology

A 12-yr integration of the coupled model was carried out. The atmospheric initial conditions were from January of a long atmospheric simulation with observed SST. The ocean initial condition was obtained by a 3-yr ocean spinup beginning from Levitus (1982) climatological January temperature and salinity, using the climatological wind stress obtained from the ECMWF analysis. The last 6 yr of the integration were used to define the coupled model climatology.

The coupled model climatology has some obvious errors in the simulation of the climatology of the tropical Pacific. The annual-mean SST in the low-latitude Pacific is shown in Fig. 2. The model is too warm throughout the Tropics, with the errors exceeding 5°C in the eastern Pacific. Because of these errors, the magnitude of the simulated SST difference between the western and eastern equatorial Pacific is only about 40% of the observed. The annual-mean zonal wind stress is also only about 40% of the magnitude of the observed. The annual-mean precipitation is too far to the south of the equator in the eastern equatorial Pacific, so that the coupled model has the familiar double ITCZ syndrome (Mechoso et al. 1995).

The climatological evolution of the simulated SST in the equatorial Pacific is shown in Fig. 3, both with and without the annual mean. The phase in the eastern Pacific near 100°W is realistic. The amplitude of the annual cycle in the eastern Pacific is only about 50% of the observed, and the amplitude in the western Pacific is unrealistically large. The annual cycle of NINO3 (5°S–5°N, 150°–90°W) SST is also about half the amplitude of the observed and the phase is shifted 2 months earlier than observed. The amplitude of the equatorial zonal wind stress annual cycle is also only about half of the observed amplitude. The double ITCZ problem persists throughout most of the year.

The annual-mean climatological error, coupled model minus assimilation, in the temperature vertically averaged over the top 235 m (referred to as ''heat content'' in the following), which is approximately proportional to the error in the thermocline depth, is shown in Fig. 4. The coupled model produces a thermocline that is too shallow throughout most of the tropical Pacific. The largest errors are in the western Pacific. The vertical structure of the error in the simulated temperature along the equator is shown in Fig. 5. Errors near the surface are relatively small. However, the temperature errors exceed 9°C at 100-m depth near the dateline. The depth of the 20°C isotherm is realistic in the eastern Pacific but is simulated to be 80 m in the western Pacific as opposed to 170 m in the analysis. The thermocline slopes too little and is too shallow in the western equatorial Pacific, consistent with the weak equatorial zonal wind stress and the balance between thermocline slope and wind stress expected from the equatorial zonal momentum equation (Schneider et al. 1995).

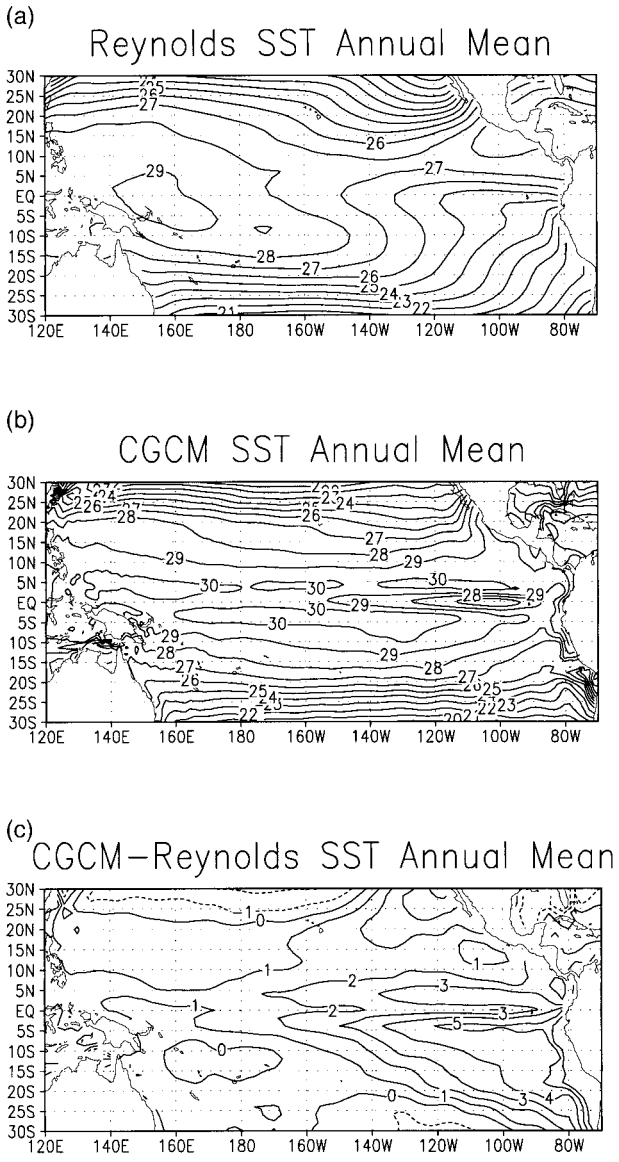

FIG. 2. (top) Climatological annual mean SST in degrees Celsius from observations (Reynolds 1988), (middle) coupled model, and (bottom) difference, coupled model minus observed. Contour interval 1°C.

One feature of the coupled model climatology is realistic. The interannual variability in the eastern equatorial Pacific SST of this short integration is strong with many realistic features. Figure 6 shows the equatorial Pacific SST anomalies relative to the 6-yr climatology for the last 9 yr of the 12-yr coupled integration. Peak warm and cold event anomalies averaged from 2°S to 2°N exceed 4°C. The largest anomalies are generally in the far eastern Pacific, except for the strong cold event in year 12, which has peak amplitude near 160°W. The standard deviation of the simulated NINO3 SST anomalies is about 1°C, somewhat larger than the 0.8°C observed amplitude. The SST anomalies vary on inter-

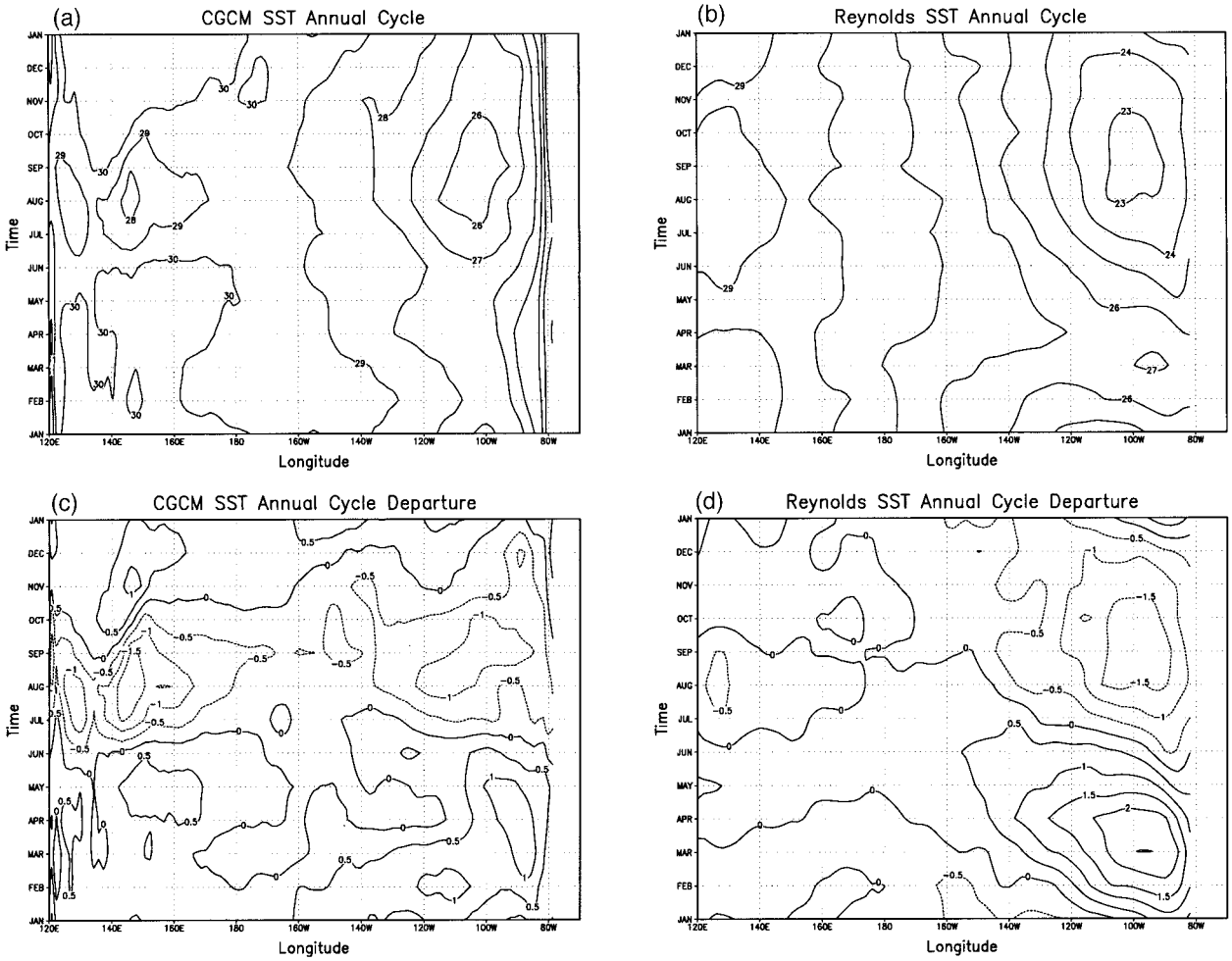

FIG. 3. Climatological evolution of SST averaged from 2°S to 2°N. (upper left) Coupled model with annual mean included, contour interval 1°C. (upper right) Observations with annual mean included, contour interval 1°C. (lower left) Coupled model with annual mean removed, contour interval 0.5°C. (lower right) Observations with annual mean removed, contour interval 0.5°C.

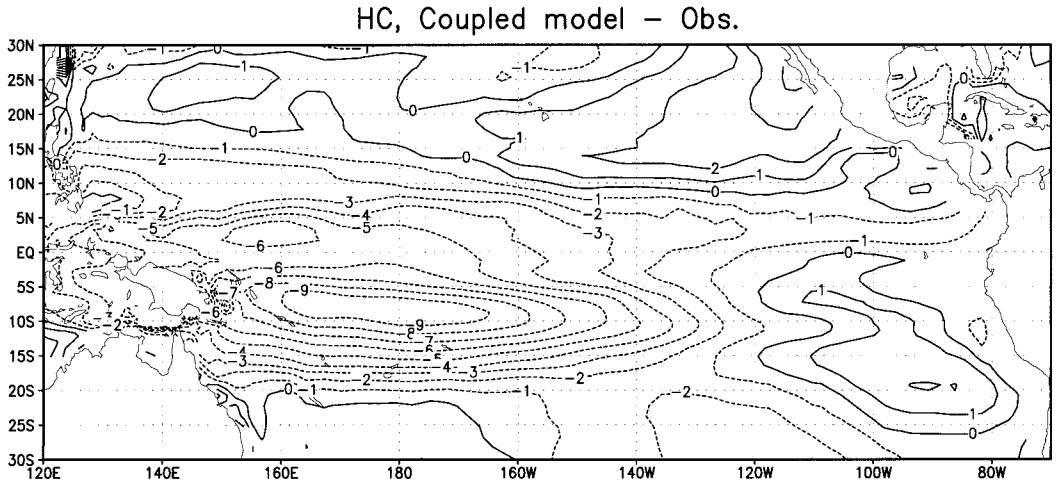

FIG. 4. Difference of the climatologies of temperature vertically averaged over the top 235 m of the ocean; coupled model minus ocean data assimilation. Contour interval 1°C.

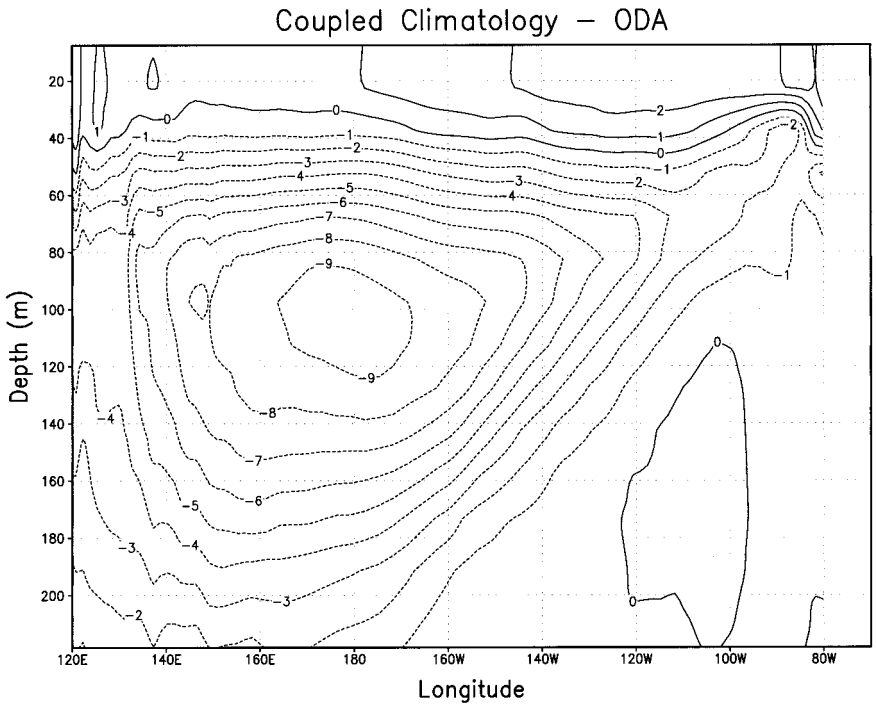

FIG. 5. Difference of the climatologies of temperature at the equator in the top 235 m of the ocean; coupled model minus ocean data assimilation. Contour interval 1°C.

annual timescales and show little systematic phase propagation, consistent with the delayed oscillator mechanism. The standard deviation of simulated NINO3 SST has an annual cycle similar to the observed but with the phase shifted 2 months earlier than observed, corresponding to the shift in the annual cycle of SST.

4. Initial conditions

The initial conditions for the ocean were created by adding the anomalies obtained from the ocean data assimilation analysis described in section 2 and appendix A to the coupled model climatology. Before beginning a coupled hindcast, the atmosphere was allowed to come to equilibrium with the initial SST anomaly by a 1-month spinup. As discussed in the introduction, the purpose of this procedure is to reduce the shock due to initial imbalance between the oceanic state and the atmospheric forcing, while allowing information from the subsurface data contained in the ocean data assimilation to influence the hindcasts. The anomaly initial condition approach provides an alternative to the more common procedure of using the full analysis of the initial state of the ocean, climatology plus anomalies, while employing flux correction and anomaly coupling to reduce the impact of climate drift and initial shock.

The atmospheric model was spun up to near balance with the initial SST by a 1-month integration with specified SST, as in Latif et al. (1993). The SST was the time-varying coupled model climatology plus the SST anomaly of the initial time for the coupled hindcast. The atmospheric spinup integration began 1 month in model time prior to the initial time for the coupled hindcast. Four initial states for the atmosphere for this spinup, one for each season, were taken from the coupled model climatology run. The justification for this procedure is that the memory of the coupled system for the ENSO variability is contained in the anomalous thermal structure of the ocean. It is important that the initial state for the atmosphere be in balance with the ocean initial condition so that this memory is not wiped out by spurious transients generated by an unrealistic imbalance.

This conceptual picture is supported by our initial tests of the coupled prediction system. The series of experiments reported here was performed first without the atmospheric initialization. An initial shock was evident case by case in the form of a prominent eastward-propagating signal. The shock originated in the western Pacific at the beginning of each hindcast and crossed the Pacific in a few months, with approximately the phase speed of an equatorial Kelvin wave signal. This is the expected mode of adjustment of the ocean to an imbalance in the initial state, and should affect the SST and evolution of the coupled system after the signal reaches the eastern Pacific. The crude atmospheric initialization greatly reduced the initial shock. As will be demonstrated below, forecasts made without the atmospheric initialization were not more skillful than a persistence forecast after a few months, while the fore-

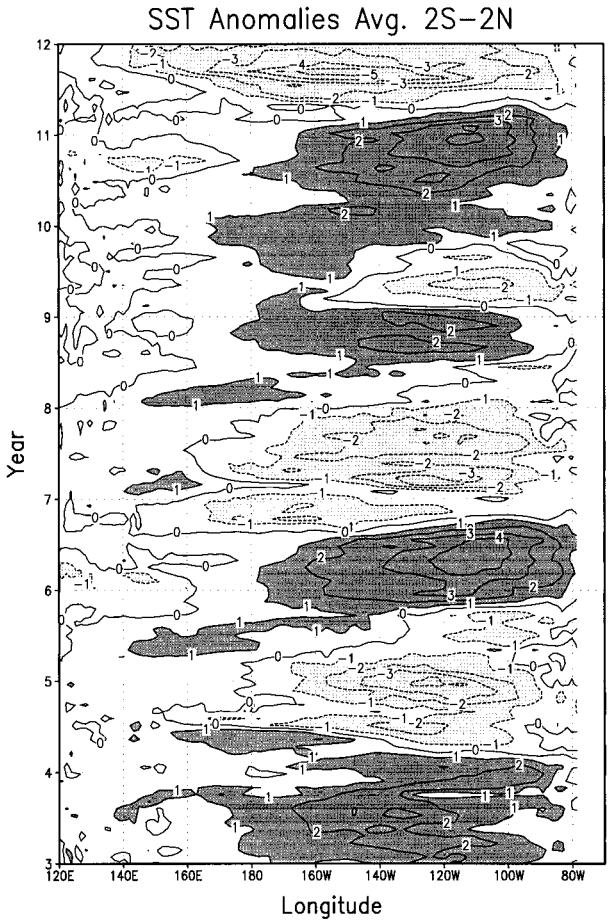

FIG. 6. SST anomalies averaged from 2°N to 2°S in the coupled integration for years 4 through 12 relative to the climatology of the last 6 yr. Contour interval 1°C. Shading as in Fig. 1.

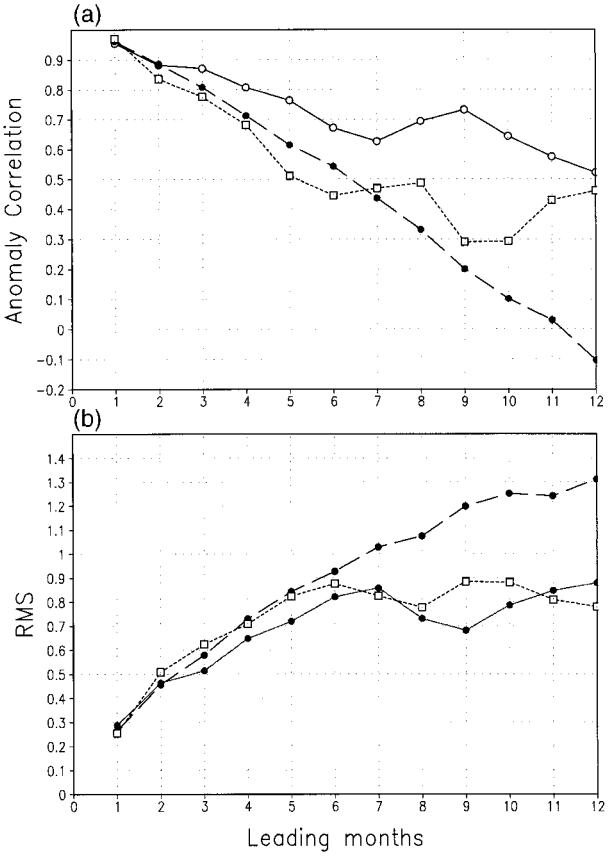

FIG. 7. (top) Anomaly correlation and (bottom) rms error (°C) of the average SST in the NINO3 region (5°S–5°N, 150°–90°W) as a function of lead time. Circles and solid line: with atmospheric initialization; squares and dashed line: without atmospheric initialization; circles and long dashed line: persistence.

casts made with atmospheric initialization were significantly better.

5. Hindcast experiments

A series of 28 12-month hindcast experiments, starting with ocean initial conditions from the end of January, April, June, and September of each year from 1986 to 1992 was performed. The approach was by and large successful in hindcasting the anomalies during this period. Also, a mean forecast error, or systematic error, develops, and a posteriori corrections produce some apparent improvement in the measures of forecast skill. In this section, we document the skill of the system, discuss the systematic error, and show case studies of the hindcasts.

a. Hindcast statistics

The anomaly correlations and rms errors of the SST anomalies averaged over the NINO3 region are shown in Fig. 7. Also shown are the results from the same 28 cases, but without the atmospheric initialization. The cases without the initialization used a slightly different atmospheric model, which did not include the changes to the cloud scheme discussed in section 3a. The earlier version of the coupled model had a similar SST annual mean and annual cycle climatology, except that it was slightly cooler in the western Pacific. When atmospheric initialization was used, there was a significant reduction in initial shock that must be due to the initialization, since the clouds were internally consistent in the models used for the climatology and hindcasts in each set of cases. A case-by-case comparison of the forecasts (not shown) indicates that improvement is traceable to reduction of the initial shock. Both sets of model results include an a posteriori systematic error correction (see section 5b). The anomaly correlations and rms errors obtained by persisting the same set of initial anomalies is also shown for reference. The anomaly correlation for the coupled hindcasts exceeds 0.6 up to almost 10 months lead time with the atmospheric initialization. Without the atmospheric initialization, the decay of the hindcast anomaly correlation with lead time is compa-

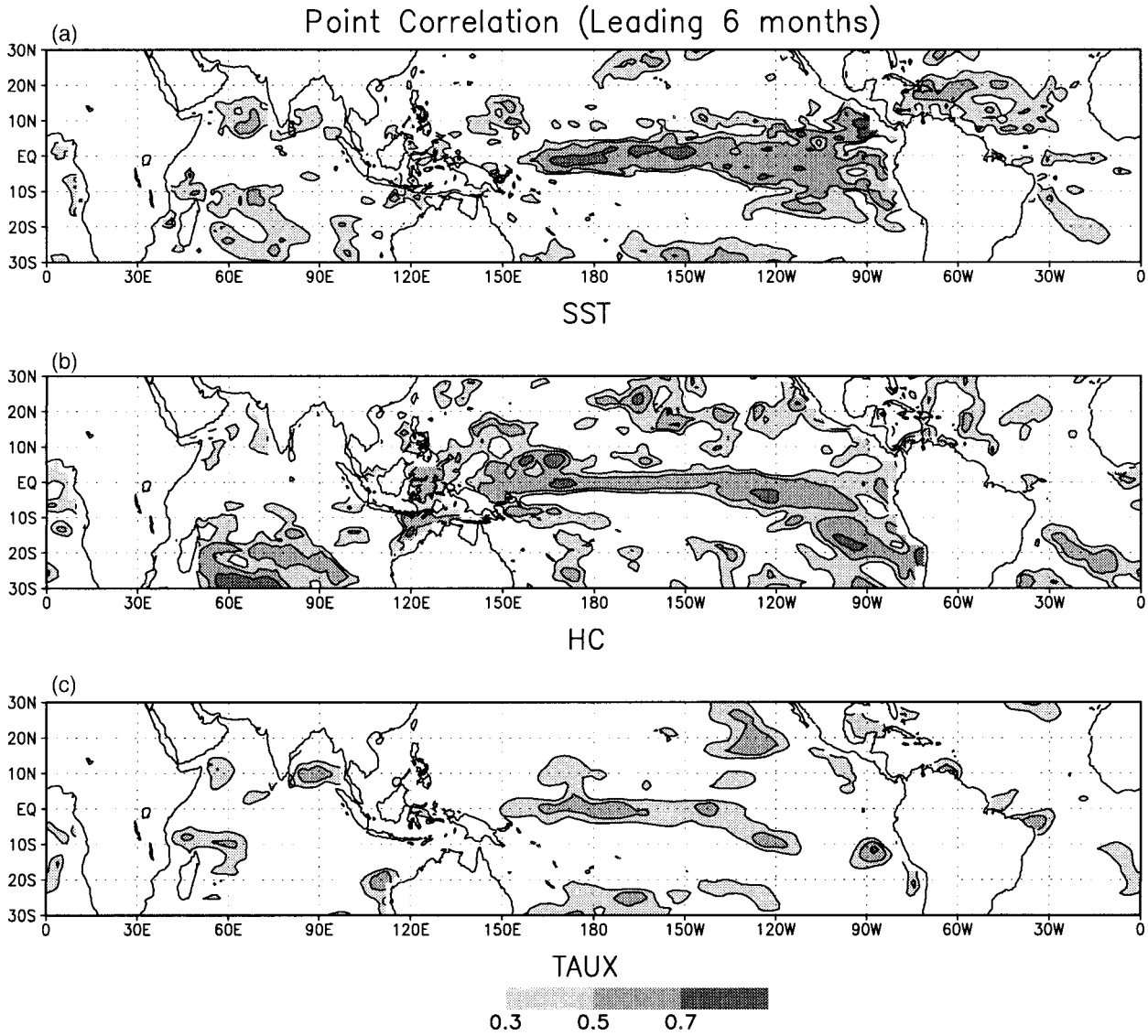

FIG. 8. Correlation of hindcast and analyzed anomalies at 6-month lead time for (top) SST, (middle) heat content, and (bottom) zonal wind stress.

rable to the behavior of persistence forecasts. The rms errors of the hindcasts with the atmospheric initialization are less than those of the hindcasts without the initialization for most lead times. The anomaly correlations with and without the atmospheric initialization differ significantly by a statistical test (see appendix B).

Point correlations between the hindcast and analyzed SST, heat content, and zonal wind stress anomalies at 6-month lead time are shown in Fig. 8. The wind stress analysis is the field derived from ECMWF surface winds used as a boundary condition for the ocean data assimilation. The SST correlations are high throughout the equatorial Pacific, except in the far west. The heat content correlation is high in a narrow strip straddling the equator stretching across the entire Pacific. This behavior of successful SST hindcasts is consistent with the delayed oscillator mechanism for ENSO variability (Suarez and Schopf 1988; Battisti and Hirst 1989), since the memory of the coupled system at the equator on intermonthly and longer timescales is contained in the heat content averaged across the Pacific (Schneider et al. 1995). The correlation for zonal wind stress anomalies in the central equatorial Pacific is also high, implying successful hindcasts of the sign of the east–west slope of the equatorial Pacific heat content anomalies, due to the balance between zonal wind stress anomalies and east–west heat content slope on ENSO timescales. The high correlations for the heat content anomalies between 5° and 10° from the equator in the far western Pacific is consistent with successful hindcasts of the

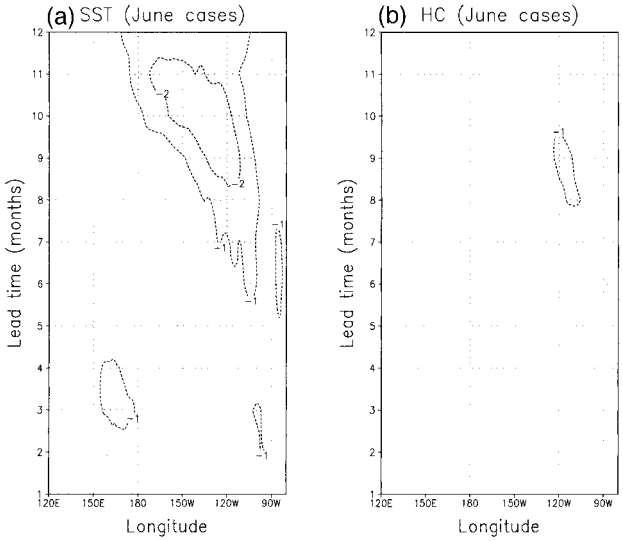

FIG. 9. Longitude (abscissa)/lead time (ordinate) sections of the average from 2°S to 2°N of the mean error relative to the coupled model climatology for the seven hindcast experiments beginning from Jun initial conditions: (left) SST, (right) heat content. Contour interval 1°C.

westward propagating Rossby waves in these regions. The zonal wind stress anomaly correlation is high just to the east of these regions, as would be expected from the delayed oscillator picture. The delayed oscillator mechanism suggests that given the delayed influence of the western Pacific Rossby waves on the eastern Pacific SST, extended predictability of the eastern Pacific SST is strongly dependent on the successful initialization and prediction of heat content anomalies in the western Pacific. It is also interesting to note from Fig. 8 that the scheme was not successful in hindcasting SST, heat content, or wind stress anomalies in the equatorial Atlantic and Indian Oceans, despite the global data assimilation. Whether this failure is due to model problems, inadequate subsurface ocean data, or inherent unpredictability remains to be investigated.

b. Systematic error

The systematic error is defined as the difference of the climatology of the hindcasts from the coupled model climatology or, equivalently, as the mean hindcast error. While the hindcast anomalies are not directly compared to the analysis anomalies, the mean analysis anomaly is zero by construction. The systematic error was computed for each seven-case ensemble of hindcasts with initial conditions from a specific month and was removed from the results shown in Fig. 7. This procedure is similar to that employed by Rosati et al. (1997) and Stockdale (1997). The evolution of the systematic error at the equator for the cases with June initial conditions is representative and is shown in Fig. 9. There is a cooling in SST that reaches a maximum of slightly more than 2°C at 9–11 months lead time. The heat content shows a small systematic cooling in the eastern Pacific. The systematic errors for the cases with April, September, and January initial conditions are broadly similar in structure and amplitude to that found in the June initial condition cases. The systematic error for the September cases is slightly larger for earlier lead times than the others, with a 2°C cold bias at 6 months lead time near 120°W, and remaining at that level out to 12 months lead time. Since only seven cases are included in the systematic error evolution calculation for each season's initial conditions, and the hindcast error grows in time, some systematic error is to be expected.

Climate drift is probably not an important component of the systematic error. The coupled model climatology comes from years 6–12 of a coupled simulation. Although the initialization procedure removes most of the climate drift, the coupled model climate has not reached equilibrium in this short a simulation. However, the rate of climate drift in the coupled simulation is negligible compared to the rate of growth of the systematic error shown in Fig. 9.

For comparison, Fig. 10 shows the difference of the mean of the seven-case June ensemble, anomalies plus climatology, from the analysis, a field that we will term the ''absolute error.'' The differences are large, with model SST more than 4°C too warm in the eastern equatorial Pacific at 7 months lead time (January). The heat content has comparably large differences from the analysis, being too cold by as much as 6°C in the western Pacific. The annual cycle of the absolute error is also large. Despite these large errors, the coupled model is able to hindcast the anomalies with some success.

Figure 11 compares the anomaly correlations and rms errors for the hindcasts with and without the removal of the systematic error. The systematic error removal produces an increase in the anomaly correlations. The analysis in appendix B indicates that this increase is significant at better than the 68% level for lead times of 8–12 months. The effect of the systematic error removal on the rms errors is pronounced. Without the systematic error removal the rms error curve has a large variability with lead time, while removing the systematic error leads to a smoother, more consistent evolution of the rms error, which in general is less than when the systematic error is not removed. The fact that the systematic error correction procedure produces significant changes in the verification scores could result from undesired correction of the nonsystematic forecast error if the number of cases is too small (e.g., consider a sample size of one). However, the system is designed so that the mean forecast should approach the model climatology for an adequate sample of cases, and the a posteriori systematic error correction should then disappear.

c. Case studies

Some successful hindcasts for equatorial Pacific SST, heat content, and zonal wind stress anomalies for spe-

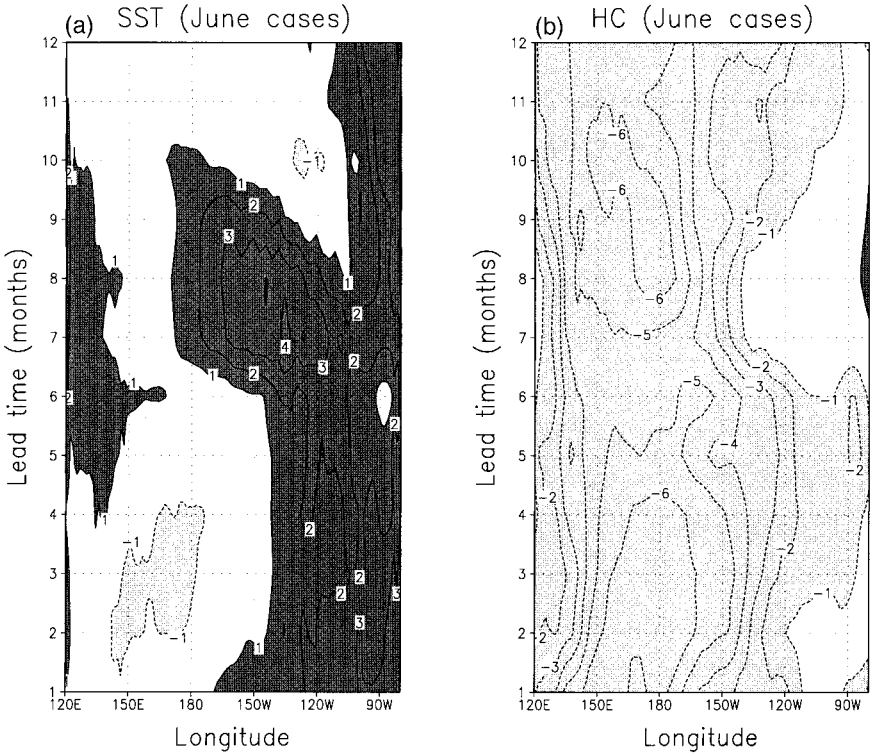

FIG. 10. Longitude (abscissa)/lead time (ordinate) sections of the average from 2°S to 2°N of the mean error relative to the analysis for the seven hindcast experiments beginning from Jun initial conditions: (left) SST, (right) heat content. Contour interval 1°C.

cific cases are compared to the analyzed anomalies in Figs. 12–15. The systematic error has been removed from the results before plotting. The evolution in Fig. 12 illustrates the growth and maintenance of a warm anomaly in the eastern Pacific beginning from the January 1987 analysis. The initial configuration of warm SST and heat content in the eastern Pacific SST, cold heat content in the western Pacific, and positive wind stress anomalies in the central Pacific is maintained through the first half of the hindcast. The observed decay of the eastern Pacific SST anomaly beginning in November 1987 is hindcast a few months too early, although the heat content shows a similar evolution to the analysis in the latter stages of the year. The hindcast wind stress anomalies occur in about the observed latitude band with a slightly weak magnitude. There is some evidence of initial shock in this hindcast, although much less pronounced than in the cases without atmospheric initialization, in the eastward propagation of a relatively cold heat content anomaly that reaches the eastern boundary between May 1987 and June 1987. No corresponding feature is present in the analysis. This shock causes some cooling in the eastern Pacific, but the disturbance is not strong enough to cause the hindcast to fail immediately.

The January 1988 initial condition case shown in Fig. 13 is one in which a cold SST anomaly grew and was maintained in the eastern Pacific in reality. The hindcast also produced this type of evolution. Warm heat content anomalies develop in the analysis in the western Pacific. Warm heat content anomalies also develop in the hindcast, but slightly later. The hindcast zonal wind stress anomalies are well placed, but slightly weaker than observed. There is little evidence of an initial shock in the heat content anomaly in this case.

The case shown in Fig. 14 starts from the January 1992 initial state. Both the hindcast and analysis evolve similarly in all fields, with warm SST anomalies in the eastern Pacific giving way to cold SST anomalies, general eastward propagation of cold heat content anomalies, and early decay of the zonal wind stress anomalies.

Figure 15 shows a less successful case, beginning from June 1991 initial conditions. While both the hindcast and analysis SST warm and then decay, the timing is very different. An initial shock can be seen in the hindcast heat content anomaly (cold anomaly at 140°E in July 1991; 170°E in August 1991; 110°W in October 1991), similar to the one in Fig. 12, but the eastern Pacific SST hindcast errors develop before the shock can influence the SST there.

The structure of the anomalies hindcast from January initial conditions is compared to the analysis for the mature warm event of July 1987 (Fig. 16) and the mature cold event of July 1988 (Fig. 17). The structure and

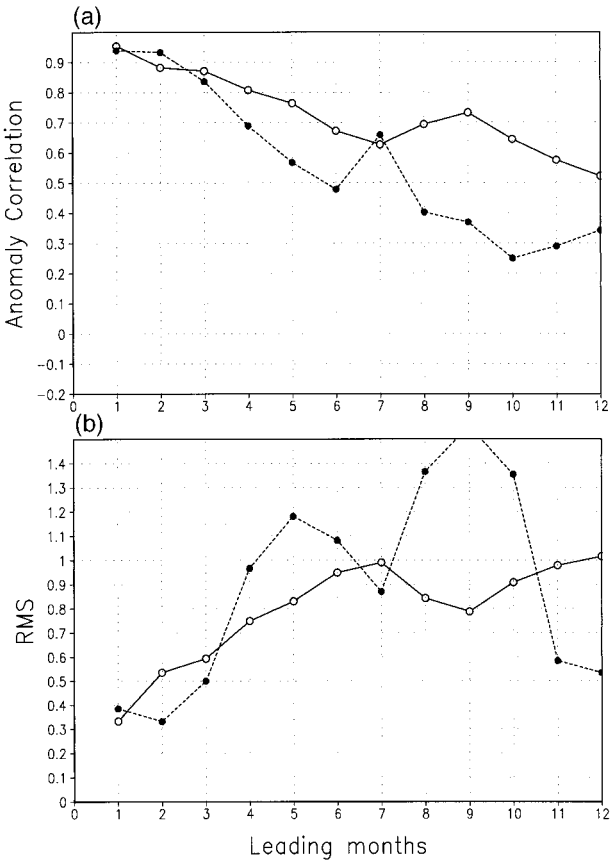

FIG. 11. (top) Anomaly correlation and (bottom) rms error (°C) for the coupled model hindcasts without removal of the systematic error (dotted line, filled circles) and with systematic error removed (solid line, open circles).

amplitude of the hindcast SST anomalies in the eastern Pacific resemble the analysis in both cases. However, the warm event hindcast SST anomaly does not extend far enough to the east, and the cold event hindcast SST anomaly does not penetrate far enough to the west. The hindcast wind stress anomalies in the equatorial eastern Pacific are approximately in the same direction as the analysis. Off the equator the hindcast wind stress anomalies have little resemblance to the analyzed ones.

6. Summary

A coupled model ENSO prediction system that uses a global coupled atmosphere–ocean GCM without flux corrections has been described. The problems of climate drift and initial shock are partially eliminated by using anomaly initial conditions. The anomalous ocean state found from an ocean data assimilation is added to the coupled model climatology to obtain the ocean initial condition. The atmosphere is brought into balance with this initial state by a 1-month spinup with the SST specified as the coupled model climatology plus the analyzed anomaly.

The system was tested by performing a series of 28 12-month hindcast experiments, one each season for the years of the ocean data assimilation, 1986–92. The system was found to produce generally good hindcasts of SST anomalies.

The coupled model SST climatology contains errors larger than the anomalies that are the target for the hindcasts. The coupled system can evidently tolerate significant errors in the annual mean and the annual cycle, and still capture the evolution of SST anomalies reasonably well. The amplitude and structure of equatorial heat content and zonal wind anomalies in the hindcast experiments are also tolerably realistic. It can be inferred that the coupled model is producing a realistic sensitivity of wind stress to SST anomalies and a realistic sensitivity of heat content and SST anomalies to wind stress anomalies. A realistic anomaly sensitivity should be prerequisite for producing the correct evolution of the coupled system from analyzed heat content and SST anomalies. If the sensitivity of the wind stress anomalies to SST anomalies was not realistic, the analyzed heat content anomalies would not be in the correct balance with the model-generated wind stress anomalies, and a strong initial shock would be present in the heat content, which would lead to unrealistic SST anomalies in the eastern Pacific after the first few months. Similarly, if the sensitivity of the SST anomalies to heat content anomalies was incorrect, the SST anomalies would undergo a rapid initial adjustment to the analyzed heat content anomalies, adversely affecting the wind stress and the subsequent evolution of the coupled system. If the sensitivity of SST anomalies to wind stress anomalies was unrealistic, the degradation would be similar, since realistic wind stress anomalies are a prerequisite to balance the heat content anomalies.

It has been suggested that coupled GCMs would be expected to have a difficult time predicting ENSO because they must simulate both the ENSO-related dynamics and the mean climatology about which these dynamics operate. This paper demonstrates that the situation might not be as critical as thought. Suitably initialized coupled GCMs with realistic sensitivity can make useful predictions of the ENSO-related dynamics despite having large errors in aspects of the mean climatology.

The results from this pilot study are encouraging, but there is also much room for improvement. The number of hindcasts was too small and the period was too short to draw firm conclusions as to the performance of this system relative to other systems. A more extensive verification of the system is contingent on the availability of further analyses from the ocean data assimilation. Also, while the use of anomaly initial conditions should bring the initial state closer to balance, problems directly attributable to errors in the mean state still remain. The thermocline in the coupled model equatorial western Pacific is far too shallow. A subsurface temperature anomaly in the analysis corresponds to a vertical dis-

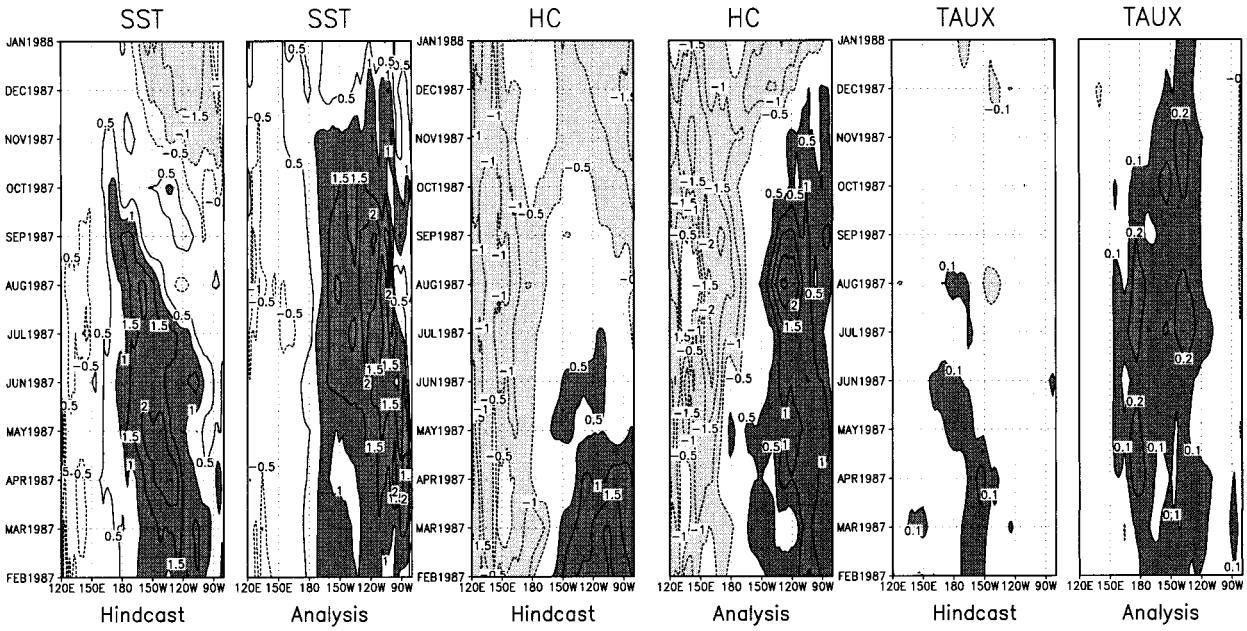

FIG. 12. Hindcast and analyzed evolution of anomalies averaged between 2°S and 2°N from Jan 1987 initial conditions. (left two panels) SST, contour interval 0.5°C; (middle two panels) heat content, contour interval 0.5°C; (right two panels) zonal wind stress, contour interval 0.1 dyn cm^{-2}.

placement of the thermocline, and therefore occurs at the correct depth of the thermocline. Adding this anomaly to the model temperature climatology will place it below the coupled model thermocline. This might cause problems by exciting the higher baroclinic vertical modes or by inducing gravitational instability.

There are some obvious paths to follow to improve the performance of the prediction system. We are concentrating on reduction of the coupled model climatological error by improving the realism of the physical parameterizations and the accuracy of the numerical approximations. We are currently carrying out hindcast experiments with a version of the coupled model in which the errors in the equatorial climatological annual

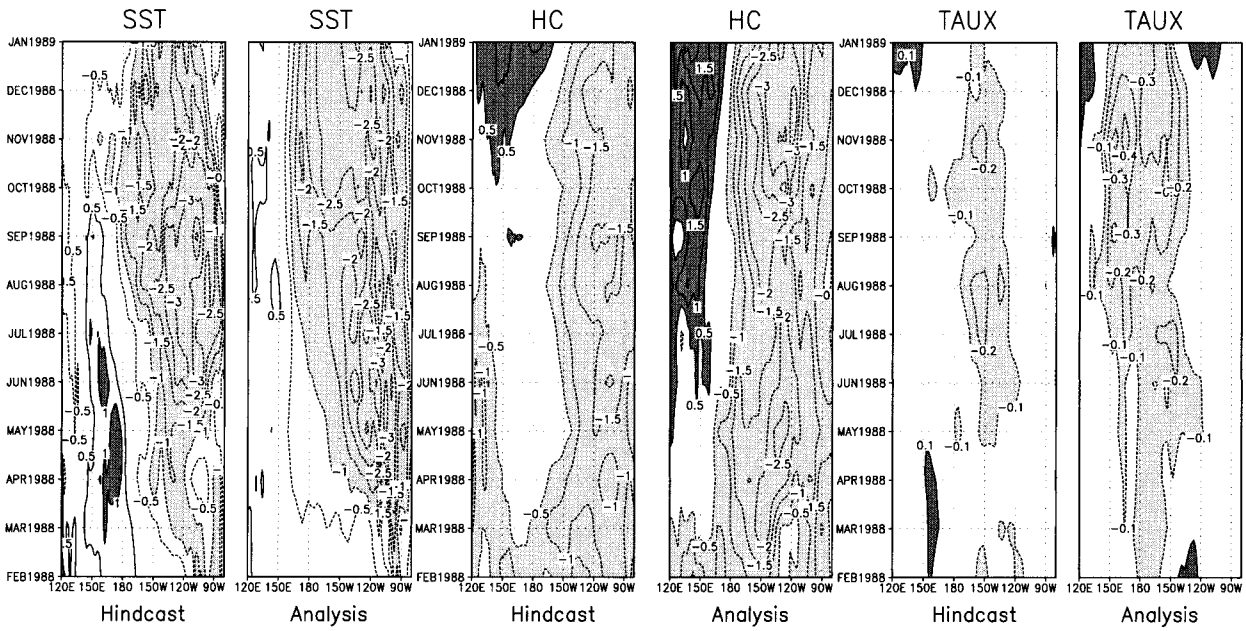

FIG. 13. As in Fig. 12 but for Jan 1988 initial conditions.

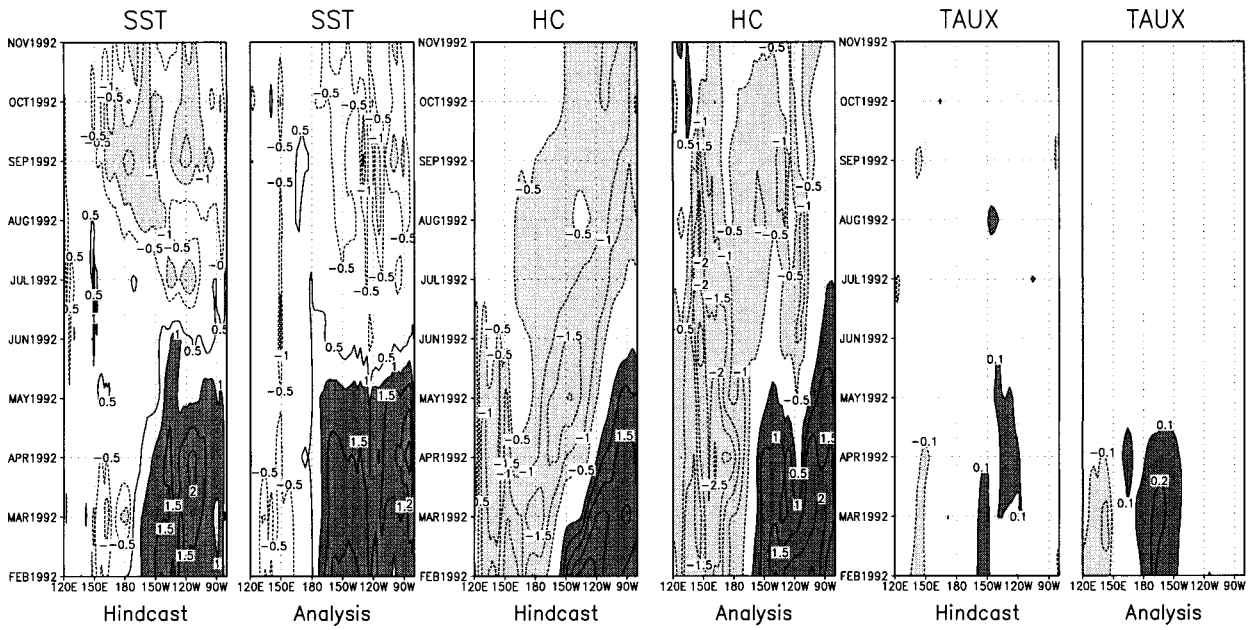

FIG. 14. As in Fig. 12 but for Jan 1992 initial conditions.

cycle of SST have been greatly reduced by improvements in the parameterization of low-level clouds (Dewitt and Schneider 1999). Preliminary indications are that the forecast error is reduced in this model. These experiments should help elucidate the sensitivity of hindcasts to reduction in the errors of the model climatology and will be reported in due course.

Acknowledgments. We are grateful to N. Pinardi of Istituto per lo Metodologie Geofisiche Ambientale and A. Rosati of the Geophysical Fluid Dynamics Laboratory, who graciously provided the optimal interpolation data assimilation system. We thank S. Levitus of the National Oceanographic Data Center, A. Leetmaa, M. Ji, and R. Reynolds of the National Centers for Environmental Prediction, and M. McPhaden of the Pacific Marine Environmental Laboratory for providing the observational datasets and oceanic reanalyses. We also

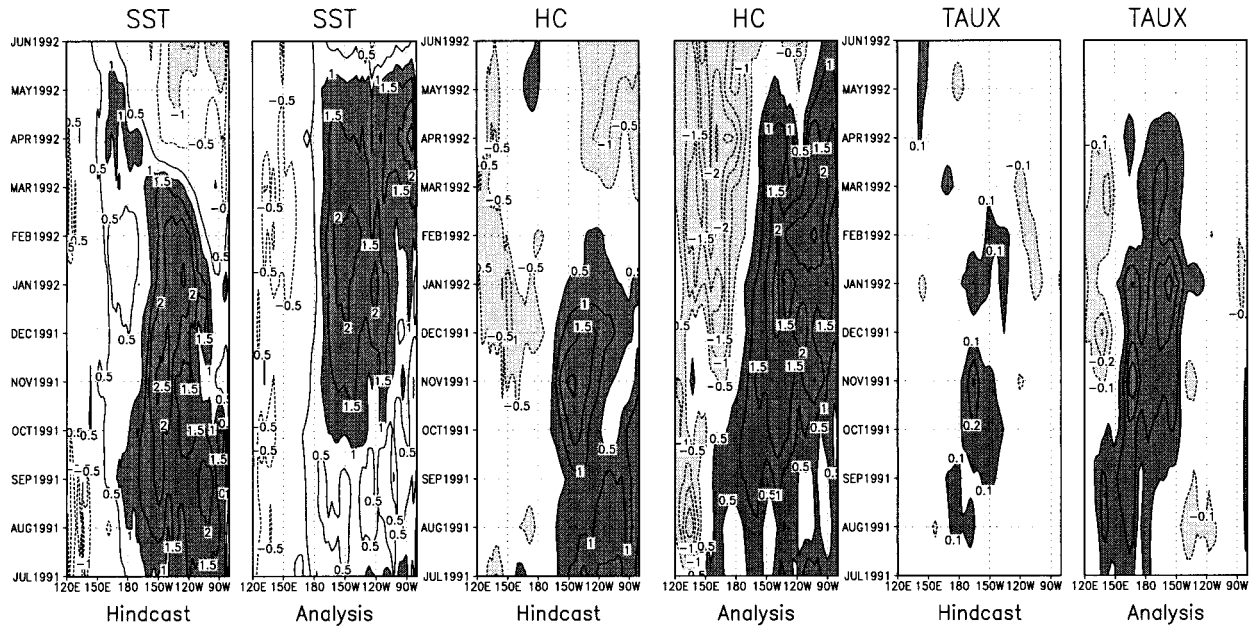

FIG. 15. As in Fig. 12 but for Jun 1991 initial conditions.

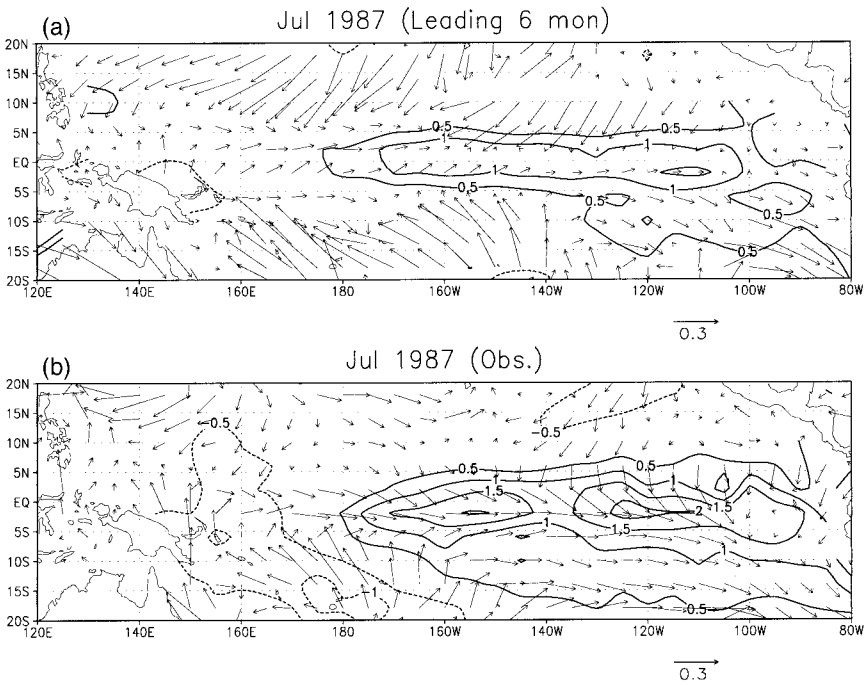

FIG. 16. (top) Hindcast from Jan 1987 initial conditions and (bottom) analysis for Jul 1987. SST anomalies: contours, interval 0.5°C. Wind stress anomalies: arrows, length corresponding to 0.3 dynes cm^{-2} displayed below each panel.

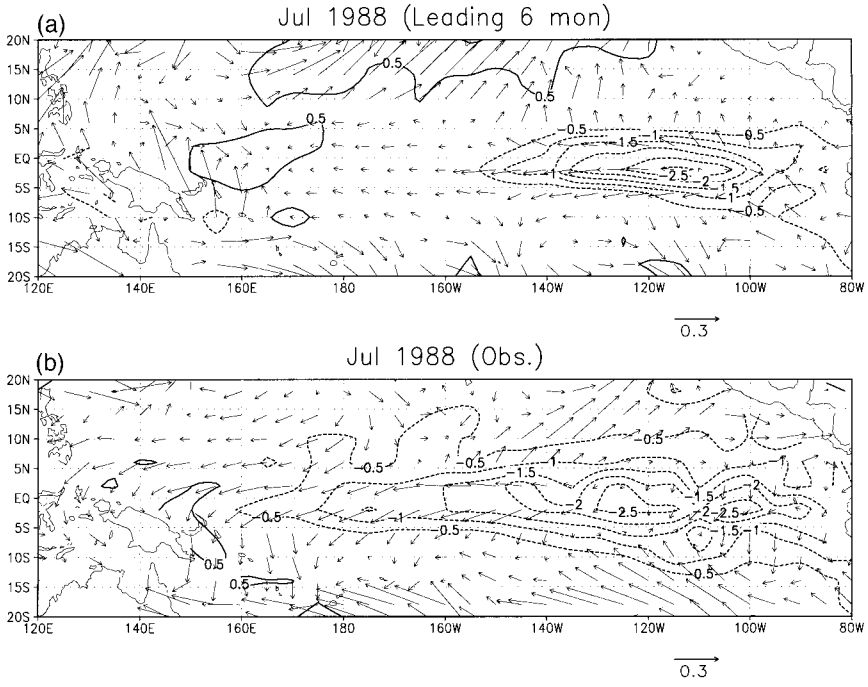

FIG. 17. As in Fig. 16 but for Jul 1988 hindcast from Jan 1988 initial conditions, and analysis.

thank Drs. K. Miyakoda, P. Schopf, and O. Alves for their suggestions on improving the manuscript. This research was supported by the National Science Foundation (ATM-9321354), the National Oceanic and Atmospheric Administration (NA26-GP0149, NA46-GP0217), and the National Aeronautics and Space Administration (NAGW-5213). Computing resources were provided by the National Center for Atmospheric Research Scientific Computing Division.

APPENDIX A

The Ocean Data Assimilation System

The observational data and the data assimilation scheme are explained here. Further details can be found in Huang and Kinter (1997).

a. The ocean model

The ocean model was as described in section 3b. The model was forced by the surface wind stress and heat flux. The solar radiation was assumed to penetrate into the upper ocean with an *e*-folding depth of 12 m (slightly less than the value of 15 m used in the coupled model). The net freshwater flux at the sea surface was set to zero.

b. Observational data

The monthly mean surface wind stress was based on the four-times-daily ECMWF 1000-mb wind analysis, using the neutral drag coefficient formulation of Trenberth et al. (1990). Originally in spectral form with resolution T106, the winds were first transformed to a Gaussian grid with zonal resolution of 1.125° and a meridional resolution ranging from 1° to 1.5°. Then the instantaneous wind stress was calculated in each grid cell and averaged within each month to form the monthly mean fields.

The heat flux is composed of radiative, sensible, and evaporative components. The radiative fluxes are divided into solar and longwave radiative parts. At each time step of the model integration, the solar radiation was prescribed by a linear interpolation of the climatological monthly means analyzed by Oberhuber (1988) from the Comprehensive Ocean Atmosphere Data Set. The other components were parameterized as functions of the model SST and prescribed surface air temperature and surface wind speed. The formulation for net longwave radiative flux was taken from Rosati and Miyakoda (1988). The sensible and latent heat fluxes were parameterized by bulk turbulent transfer formulas with parameters as given by Philander et al. (1987). The surface wind speed was derived from the instantaneous wind stress, approximately equivalent to assuming a constant drag coefficient of 1.4×10^{-3}. The surface air temperature was taken from monthly climatologies compiled by Oort (1983). The model was initialized from an ocean at rest with January climatological temperature and salinity (Levitus 1982) and spun up for 4 yr forced with the monthly mean climatological wind stress, before starting the data assimilation in January 1986.

The observations used as input to the data assimilation system are SST and temperature profiles. The SST observations were taken from the global $1° \times 1°$ CPC analysis based on in situ (ship and buoy) measurements and Advanced Very High Resolution Radiometer satellite retrievals of SST (Reynolds and Smith 1994). Except for cloudy regions, the satellite observations provide coverage of most of the world oceans in a 7-day period. The distribution of ship observations depends on shipping traffic and is most dense in the midlatitude Northern Hemisphere. The buoy data are designed to supplement the ship measurements and are mostly concentrated in the tropical Pacific Ocean.

The CPC analysis combines all available observations obtained in each 7-day interval to produce a global field, using an optimum interpolation (OI) scheme with a first-guess field that is the analysis for the preceding week. Before the analysis, satellite biases relative to the in situ data are corrected using the Poisson equation (Reynolds 1988; Reynolds and Marsico 1993). The analysis may not be reliable in data sparse areas, where persistence is assumed. However, considering the coverage of satellite measurements, this situation is infrequent and mostly near the ice edge. Otherwise, the resulting analysis should not be sensitive to the specific OI method. In fact, features of the high-resolution satellite observations are well preserved in the analysis (Reynolds and Smith 1994).

The temperature profiles were from two sources. One is a set of profiles in the World Ocean Atlas 1994 CD-ROM series (Levitus and Boyer 1994) with some more recent updates. These profiles are from the National Oceanographic Data Center (NODC) master archives, as well as from the results of two projects: the National Oceanographic Data Archaeology and Rescue and the Global Oceanographic Data Archaeology and Rescue. These measurements were collected throughout the world oceans during 1900–92 using a variety of instruments, including expendable bathythermographs (XBT); conductivity, temperature, and depth profilers; salinity, temperature, and depth profilers; bathythermographs; and mechanical bathythermographs. Corrections of the depth error associated with the drop rate problem for several kinds of XBTs (Barnes and Sessions 1984; Hanawa and Yoritaka 1987; Wright and Szabados 1989; Singer 1990; Hallock and Teague 1992) are made at NODC. Levitus and Boyer (1994) checked the profiles for unreasonable ship speed between measurements, temperature or density inversion, data duplication, as well as other unrealistic features in comparison to the climatological field and its seasonal standard deviations. Every profile is flagged with the result of each quality control check. The data are provided in two sets;

one is the original profiles, the other is profiles interpolated to standard level depths defined by NODC (Levitus 1982). In this study, we have used the profiles at standard NODC levels that passed all the quality control requirements.

The other data source is the coupled modeling group of the National Centers for Environmental Prediction (NCEP), which provides XBT profiles for the Atlantic and Pacific Oceans taken since 1980. Measurements from thermistor chain moorings of the Tropical Ocean Global Atmosphere Tropical Atmosphere Ocean array have also been added since 1989. Error checking and correction have been carried out at NCEP for each profile through a series of objective and subjective procedures (Ji et al. 1995). However, there is no drop rate correction as is done for the NODC data. In this study, we used the NCEP data as a complementary set to the NODC data.

There were substantial duplications between these two datasets. For most months in the 1980s there are many more temperature profiles in the NODC than in the NCEP dataset. Apart from a general increase of observations in the ship tracks, the additional data from NODC are mainly in the western boundary currents of both the northern Atlantic and Pacific Oceans, as well as in the Indian Ocean and the Mediterranean Sea. The latter are not covered by the NCEP data. However, the NCEP data are not just a subset of the NODC data.

During the 1990s, the number of observations in the NODC CD-ROMs has been decreasing significantly due to the time lag in compiling and assuring the quality of the new measurements. On the other hand, as a part of an operational forecast system, the NCEP dataset is relatively more up to date since observations are obtained directly through the Global Telecommunications System (GTS). Therefore, after 1990, the NCEP dataset generally contains more observations than the corresponding NODC CD-ROMs although the quality of the former may not be as thoroughly checked.

In producing a unified dataset from these two sources, we have used the following procedure. First, duplications between these two datasets were eliminated. A profile was considered a duplicate if it fell in the same square of the ocean GCM (OGCM) grid cell with another profile obtained within the same day. In such a case, the NCEP profile was eliminated. All the remaining profiles were then interpolated linearly to corresponding model levels. After the interpolation, several further quality control steps similar to those done at NODC were repeated, including a temperature inversion check as well as a check that the observations were within a reasonable range of the Levitus and Boyer (1994) monthly climatology and seasonal standard deviation. This procedure provides a common criterion for profiles from the two sources, which went through somewhat different prior quality control procedures. It also eliminates possible improper features created in the vertical interpolation. In practice, few profiles are eliminated through this procedure. Finally, a topography check was conducted to make sure that no data were on land or below the bathymetry relative to the model grids.

c. Data assimilation scheme

The ocean data assimilation scheme is the same as that described in Derber and Rosati (1989). It is a univariate, variational optimum interpolation of temperature only, in which the first guess is provided by the OGCM. The observations are inserted into the ocean model integration by computing a temperature correction field derived from the optimum interpolation equation, which is formulated using a variational approach recommended by Lorenc (1986), among others. The variational approach involves minimizing a cost function with two terms, one associated with the fit of the objective analysis to the model field, and the other with the fit of the analysis to the observed field. The cost function J may be written

$$J = (T - T_f)^{\mathrm{T}}\mathbf{E}^{-1}(T - T_f) + (\mathbf{D}(T) - T_0)^{\mathrm{T}}\mathbf{F}^{-1}(\mathbf{D}(T) - T_0), \quad \text{(A1)}$$

where T is the analyzed temperature vector and T_f is the first guess temperature vector, $\mathbf{D}$ is a transformation matrix (usually a spatial interpolation operator), and T_0 is the vector of temperature observations. The model error covariance matrix $\mathbf{E}$ is specified assuming a Gaussian-like distribution of the horizontal covariance (Derber and Rosati 1989). Its e-folding spatial scale is prescribed as 570 km near the equator and gradually decreasing with latitude, as in Derber and Rosati (1989). This value may be too coarse in the meridional direction, since the equatorial Rossby radius is on the order of 2°. Assuming the observational errors are not spatially correlated, the observational error covariance matrix $\mathbf{F}$ is diagonal. The functional (1) is minimized using the preconditioned conjugate gradient algorithm through an iterative procedure (Navon and Legler 1987; Derber and Rosati 1989). A maximum of three iterations are made. The model temperature is updated through the assimilation procedure only for the levels above 300 m.

The assimilation can, in principle, be conducted continuously accompanying the OGCM integration. This approach, however, is quite costly. As an alternative, we performed the assimilation only for the first 12 h of each day of model integration, following Rosati et al. (1995). The correction derived from the last assimilation step on a given day was reinserted into the model field at every time step for the rest of the day. The actual times of the assimilation, then, were dependent on the model time step. Moreover, a 30-day window was used in the assimilation so that the temperature correction at a given instant included observations within ± 15 days of that instant. The contribution of each observation was weighted by the diagonal element of $\mathbf{F}^{-1}$ that is the reciprocal of the observational error variance multiplied

by a factor linearly dependent on the length of the time interval between the instant of the observation and that of the assimilation. The smoothing applied to the wind stress (monthly mean) and subsurface data (30-day window) are slightly different. The effect on this inconsistency in the hindcasts is probably small, given that the atmospheric initial conditions are obtained from a spinup rather than an analysis.

The observational error variance of temperature profile data was mostly assigned to be $(0.5°C)^2$, a value chosen to represent the level of instrument error. For the profiles near the northwestern Pacific and Atlantic Oceans, however, the variance was assigned to be $(1°C)^2$ to reflect the fact that mesoscale eddies observed in these areas are not resolved by the OGCM. The error variance of the SST data was also assigned to be $(1°C)^2$ since the CPC analysis is not exactly an ''observation.'' The variance of the model error, which determines the magnitude of the elements in matrix **E**, was assigned to be $(0.1°C)^2$. The smaller variance of model error was used because these errors are corrected continuously through repeated data insertion within the 30-day window.

APPENDIX B

Reliability of Results: Effect of Sample Size and Choice of Hindcast Period

An earlier version of the coupled model described above is currently being used to make experimental ENSO forecasts in real time (e.g., Kirtman et al. 1996). This other prediction system, hereafter referred to as the anomaly coupled model, is described in detail in Kirtman et al. (1997) and briefly summarized below. Given that the anomaly coupled model has been validated over a much larger sample of hindcasts cases and shown to be competitive with other state-of-the-art models, it provides a useful benchmark for evaluating the performance of the coupled model. Here, the effect on the statistics of the anomaly coupled model of using 28 case subensembles or restricting the period to the same period studied with the coupled model are examined.

a. Description of anomaly coupled system

The ocean and atmosphere components in the anomaly coupled model exchange only predicted anomalies of sea surface temperature and wind stress. The wind stress and sea surface temperature anomalies are computed relative to atmosphere and ocean model climatologies, respectively, while the climatology upon which the anomalies are superimposed is specified by observations. The model climatologies are defined by separate uncoupled extended simulations of the ocean and atmosphere models. In the case of the atmosphere, the model climatology is computed from a 45-yr (1949–94) integration with specified observed SST, and, in the case of the ocean, a 30-yr (1964–94) integration with prescribed Florida State University wind stress is used. The heat flux into the ocean in the anomaly coupled model is found by relaxation to the climatological SST.

In addition to the anomaly coupling strategy, the Kirtman et al. (1997) model uses an empirical correction to the atmospheric model wind stress anomaly developed by Huang and Shukla (1997). This empirical correction gives an improved ocean simulation (Huang and Shukla 1997; Kirtman and Schneider 1996) and improved ENSO hindcasts (Kirtman et al. 1997).

While these empirical corrections improve the wind stress and uncoupled ocean simulations, Kirtman and Schneider (1996) found that, in terms of initial conditions for coupled forecasts, improvements could still be made without a sophisticated ocean data assimilation system. They developed an iterative procedure for modifying the wind stress anomaly based on the error in the ocean model simulated SST anomaly. The main idea behind the procedure is to use the large degree of equilibrium between the zonal wind stress anomaly and the SST anomaly in the tropical Pacific to iteratively modify the zonal wind stress anomaly. In essence, the wind stress is assimilated, assuming SST observations are more reliable than wind stress observations. The final product is an improved ocean model simulation and better initial conditions for coupled forecasts.

The same resolution is used in the anomaly coupled and coupled model atmospheres and oceans, the same atmospheric initialization is employed, and both systems remove the systematic error a posteriori. Besides the coupling scheme, the major features of the anomaly coupled system that are different from those of the coupled system are that the atmosphere uses a modified version of the Kuo (1965) deep convection scheme, the ocean domain is restricted to the Pacific basin, and direct measurements are not incorporated into the initial conditions below the top layer of the ocean.

b. Comparison of hindcast performance

The prediction skill of the anomaly coupled model has been evaluated based on 180 hindcasts sampling the years 1965–91. Using a NINO3 SST anomaly correlation of 0.6 as a minimum threshold for useful forecasts, the anomaly coupled model produces skillful hindcasts for lead times of up to 12 months. In the sample of 180 hindcasts, there are 20 cases that overlap with the 28 hindcasts made with the coupled model. These 20 hindcasts are initialized at the beginning of February, May, July, and October of 1986–89 and 1991. The years 1990 and 1992 were not included in the set of cases examined with the anomaly coupled model because the anomalies that occurred were small. Figure B1 shows the NINO3 sea surface temperature anomaly correlation coefficient and rms error for the 20 common cases of the anomaly coupled model and coupled models. The coupled model performs better than the anomaly coupled model for lead

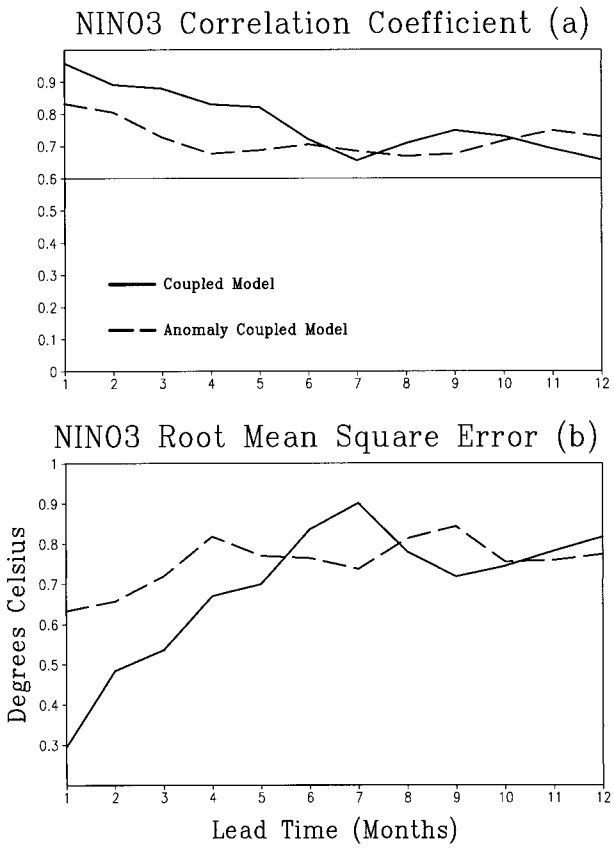

FIG. B1. Summary verification statistics of NINO3 SST indices for the 20 common hindcasts of the coupled model (solid curve) and anomaly coupled model (dashed curve) initialized in 1986–92. (top) Anomaly correlation (dimensionless). (bottom) Rms error (°C).

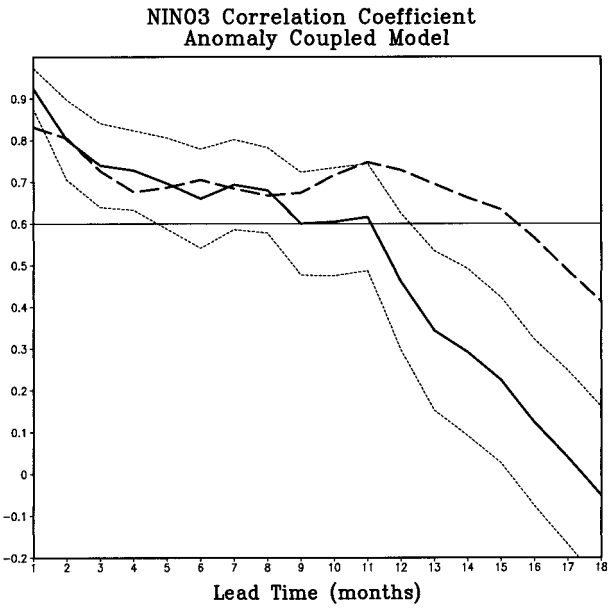

FIG. B2. Monte Carlo estimate of uncertainty in the NINO3 anomaly correlation for the anomaly coupled system. The distribution of anomaly correlations from 1000 randomly chosen 28-hindcast subsets sampling the years 1965–91 is Gaussian about the mean (solid line) with standard deviation indicated by the dotted lines. The dashed line shows the anomaly correlation from the 20 cases that were in common with the coupled system cases.

times out to 5 months. The insertion of observed subsurface data at the initial time is probably advantageous for the coupled model (Ji and Leetmaa 1997). At longer lead times, the performance of the coupled model is similar to that of the anomaly coupled model.

c. *Estimate of effects of limited sample size and choice of period*

The sample size of 28 hindcasts is rather small, a problem that is not unusual in hindcast studies with coupled GCMs, especially those without anomaly coupling. For example, the early study by Latif et al. (1993) used a sample of 20 cases from five separate years, and Rosati and Miyakoda (1997) had a sample size of 14 cases. Since the coupled model variabilty is intrinsically chaotic (see section 3d), possibly in part due to the influence of atmospheric noise, a larger sample size would be desirable to more accurately evaluate the predictability of the system. Also, the period from which the cases were drawn was limited to the 7 years for which the in-house ODA had been performed. It has been argued that the 1980s and early 1990s are a particularly easy period to hindcast (Chen et al. 1995; Ji et al. 1996). If this is true, then the verification scores are not representative of the scores that would be obtained from a longer period. For comparison, recent hindcast studies that used initial conditions from ODA covered the 7-yr period from 1982 to 1988 (Rosati et al. 1997) and the 11-yr period from 1983 to 1993 (Ji and Leetmaa 1997).

The results from the anomaly coupled model have been used to estimate the representativeness of randomly chosen 28 case samples, and whether the period used was anomalously predictable. Because of the case-by-case and aggregate similarity of the common results from the two systems, these statistics provide an estimate of the representativeness of the results of the coupled system. Figure B2 shows the mean anomaly correlation of 1000 randomly chosen 28-case samples from the anomaly coupled results. The distribution of the anomaly correlations of the individual samples forms a Gaussian cloud around the mean, represented by curves drawn one standard deviation from the mean of the 1000 samples. The uncertainty due to the small sample size is not small. From 6 to 11 months lead time, the standard deviation is 0.11. The coupled model anomaly correlation shown in Fig. B1 lies within the one standard deviation cloud of Fig. B2 for lead times longer than 5 months. Then the coupled model performance for these lead times is not statistically distinguishable from the

mean performance of the anomaly coupled model for this set of cases.

The 20-case anomaly correlation for the hindcasts made with the anomaly coupled model in common with the coupled model is also shown in Fig. B2. This curve also lies closer than one (28 case) standard deviation from the mean of the anomaly coupled system up to 11 months lead time. According to this measure, the late 1980s and early 1990s (excluding years with small anomalies) were not anomalously predictable for lead times less than 11 months, but may have been anomalously predictable for lead times of 12–18 months. Since the coupled model hindcasts were only carried out to a 12-month lead time, those cases did not benefit from the anomalous predictability.

Using the standard deviation found from the Monte Carlo simulation with the anomaly coupled model for error estimates, the hindcasts with and without atmospheric initialization (Fig. 7) differ significantly (with a confidence estimate of 68%) for 5 months and longer lead times. Also the removal of the systematic error causes a significant difference in the anomaly correlation for 5 months and longer lead times (Fig. 11).

REFERENCES

Barnes, J., and M. H. Sessions, 1984: A field performance test of the Sippican deep aircraft-deployed expendable bathythermograph. *J. Geophys. Res.,* **89,** 3615–3621.

Battisti, D. S., and A. C. Hirst, 1989: Interannual variability in a tropical atmosphere–ocean model: Influence of the basic state, ocean geometry and nonlinearity. *J. Atmos. Sci.,* **46,** 1687–1712.

Bryan, K., and L. Lewis, 1979: A water mass model of the World Ocean. *J. Geophys. Res.,* **84,** 2503–2517.

Cane, M. A., S. E. Zebiak, and S. C. Dolan, 1986: Experimental forecasts of El Niño. *Nature,* **321,** 827–832.

Chen, D., S. E. Zebiak, A. J. Busalacchi, and M. A. Cane, 1995: An improved procedure for El Niño forecasting. *Science,* **269,** 1699–1702.

Derber, J., and A. Rosati, 1989: A global oceanic data assimilation system. *J. Phys. Oceanogr.,* **19,** 1333–1347.

DeWitt, D. G., 1996: The effect of the cumulus convection scheme on the climate of the COLA general circulation model. COLA Rep. 27, 58 pp. [Available from COLA, 4041 Powder Mill Rd., Suite 302, Calverton, MD 20705.]

——, and E. K. Schneider, 1997: The Earth radiation budget as simulated by the COLA GCM. COLA Rep. 35, 39 pp. [Available from COLA, 4041 Powder Mill Rd., Suite 302, Calverton, MD 20705.]

——, and ——, 1999: The processes determining the annual cycle of equatorial sea surface temperature: A coupled general circulation model perspective. *Mon. Wea. Rev.,* **127,** 381–395.

Gill, A. E., 1982: *Atmosphere–Ocean Dynamics*. Academic Press, 662 pp.

Hallock, Z. R., and W. J. Teague, 1992: The fall rate of the T-7 XBT. *J. Atmos. Oceanic Technol.,* **9,** 470–483.

Hanawa, K., and H. Yoritaka, 1987: Detection of systematic errors in XBT data and their correction. *J. Oceanogr. Soc. Japan,* **43,** 68–76.

Huang, B., and J. L. Kinter III, 1997: A global ocean analysis for 1986–1992. COLA Rep. 38, 62 pp. [Available from COLA, 4041 Powder Mill Rd., Suite 302, Calverton, MD 20705.]

——, and J. Shukla, 1997: An examination of the AGCM simulated surface wind stress and low-level winds over the tropical Pacific Ocean. *Mon. Wea. Rev.,* **125,** 985–998.

Ji, M., and T. M. Smith, 1995: Ocean model response to temperature data assimilation and varying surface wind stress: Intercomparisons and implications for climate forecast. *Mon. Wea. Rev.,* **123,** 1811–1821.

——, and A. Leetmaa, 1997: Impact of data assimilation on ocean initialization and El Niño prediction. *Mon. Wea. Rev.,* **125,** 742–753.

——, A. Kumar, and A. Leetmaa, 1994: An experimental coupled forecast system at the National Meteorological Center. *Tellus,* **46A,** 398–418.

——, A. Leetmaa, and J. Derber, 1995: An ocean analysis system for seasonal to interannual climate studies. *Mon. Wea. Rev.,* **123,** 460–481.

——, A. Leetmaa, and V. E. Kousky, 1996: Coupled model predictions of ENSO during the 1980s and 1990s at the National Centers for Environmental Prediction. *J. Climate,* **9,** 3105–3120.

Kiehl, J. T., J. J. Hack, and B. P. Briegleb, 1994: The simulated Earth radiation budget of the National Center for Atmospheric Research Community Climate Model CCM2 and comparisons with the Earth Radiation Budget Experiment (ERBE). *J. Geophys. Res.,* **99,** 20 815–20 827.

Kirtman, B. P., and E. K. Schneider, 1996: Model based estimates of equatorial zonal wind stress. *J. Climate,* **9,** 1077–1091.

——, and D. G. Dewitt, 1997: Comparison of atmospheric model wind stress with three different convective parameterizations: Sensitivity of tropical Pacific Ocean simulations. *Mon. Wea. Rev.,* **125,** 1231–1250.

——, B. Huang, Z. Zhu, and J. Shukla, 1996: Tropical Pacific SST predictions with a coupled GCM. Experimental Long-Lead Forecast Bulletin, Vol. 5, No. 3, 14–16. [Available from Climate Prediction Branch, CPC, W/NP51 NOAA, National Weather Service, Washington, DC 20333.]

——, J. Shukla, B. Huang, Z. Zhu, and E. K. Schneider, 1997: Multiseasonal predictions with a coupled tropical ocean global atmosphere system. *Mon. Wea. Rev.,* **125,** 789–808.

Kuo, H. L., 1965: On the formation and intensification of tropical cyclones through latent heat release by cumulus convection. *J. Atmos. Sci.,* **22,** 40–63.

Latif, M., A. Sterl, E. Maier-Reimer, and M. M. Junge, 1993: Structure and predictability of the El Niño/Southern Oscillation phenomenon in a coupled ocean–atmosphere general circulation model. *J. Climate,* **6,** 700–708.

——, and Coauthors, 1998: A review of the predictability and prediction of ENSO. *J. Geophys. Res.,* **103,** 14 375–14 394.

Levitus, S., 1982: *Climatological Atlas of the World Ocean*. NOAA, NOAA Professional Paper 13, 173 pp. and 17 microfiche. [Available from U.S. Government Printing Office, Superintendent of Documents, Mail Stop: SSOP, Washington, DC 20402-9328.]

——, and T. P. Boyer, 1994: *World Ocean Atlas 1994*. Vol. 4, *Temperature,* U. S. Department of Commerce, 117 pp. [Available from U.S. Government Printing Office, Superintendent of Documents, Mail Stop: SSOP, Washington, DC 20402-9328.]

Lorenc, A. C., 1986: Analysis methods for numerical weather prediction. *Quart. J. Roy. Meteor. Soc.,* **112,** 1177–1194.

McCreary, J. P., 1978: Eastern tropical ocean response to changing wind systems. *Review Papers of Equatorial Oceanography—FINE Workshop Proceedings,* Nova N.Y.I.T. University Press, chapter 7.

Mechoso, C. R., and Coauthors, 1995: The seasonal cycle over the tropical Pacific in coupled ocean–atmosphere general circulation models. *Mon. Wea. Rev.,* **123,** 2825–2838.

Moorthi, S., and M. J. Suarez, 1992: Relaxed Arakawa–Schubert: A parameterization of moist convection for general circulation models. *Mon. Wea. Rev.,* **120,** 978–1002.

Navon, I. M., and D. M. Legler, 1987: Conjugate-gradient methods for large-scale minimization in meteorology. *Mon. Wea. Rev.,* **115,** 1479–1502.

Oberhuber, J. M., 1988: An atlas based on the COADS data set: Budgets of heat buoyancy and turbulent kinetic energy at the surface of the global ocean. Max-Planck Institut für Meteorol-

ogie Rep. 15, 199 pp. [Available from Max-Planck Institut für Meteorologie, Bundesstrasse 55, D-20146 Hamburg, Germany.]
Oort, A. H., 1983: Global atmospheric circulation statistics, 1958–1973. NOAA Professional Paper 14, U. S. Department of Commerce, 180 pp. [Available from U.S. Government Printing Office, Superintendent of Documents, Mail Stop: SSOP, Washington, DC 20402-9328.]
Pacanowski, R. C., and S. G. H. Philander, 1981: Parameterization of vertical mixing in numerical models of tropical oceans. *J. Phys. Oceanogr.,* **11,** 1443–1451.
——, K. Dixon, and A. Rosati, 1993: The GFDL modular ocean model user's guide, version 1.0. GFDL Ocean Group Tech. Rep. 2, 77 pp. [Available from GFDL/NOAA, Princeton University, Princeton, NJ 08542.]
Paulson, C. A., and J. J. Simpson, 1977: Irradiance measurements in the upper ocean. *J. Phys. Oceanogr.,* **7,** 952–956.
Philander, S. G. H., W. J. Hurlin, and A. D. Seigel, 1987: A model of the seasonal cycle in the tropical Pacific Ocean. *J. Phys. Oceanogr.,* **17,** 1986–2002.
Reynolds, R. W., 1988: A real time global sea surface temperature analysis. *J. Climate,* **1,** 75–86.
——, and D. C. Marsico, 1993: An improved real-time global sea surface temperature analysis. *J. Climate,* **6,** 114–119.
——, and T. M. Smith, 1994: Improved global sea surface temperature analysis. *J. Climate,* **6,** 929–948.
Ropelewski, C. F., and M. S. Halpert, 1987: Global and regional scale precipitation associated with El Niño/Southern Oscillation. *Mon. Wea. Rev.,* **115,** 1606–1626.
Rosati, A., and K. Miyakoda, 1988: A general circulation model for upper ocean circulation. *J. Phys. Oceanogr.,* **18,** 1601–1626.
——, R. Gudgel, and K. Miyakoda, 1995: Decadal analysis produced from an ocean data assimilation system. *Mon. Wea. Rev.,* **123,** 2206–2228.
——, K. Miyakoda, and R. Gudgel, 1997: The impact of ocean initial conditions on ENSO forecasting with a coupled model. *Mon. Wea. Rev.,* **125,** 754–772.
Schneider, E. K., and Z. Zhu, 1998: Sensitivity of the simulated annual cycle of sea surface temperature in the equatorial Pacific to sunlight penetration. *J. Climate,* **11,** 1932–1950.
——, B. Huang, and J. Shukla, 1995: Ocean wave dynamics and El Niño. *J. Climate,* **8,** 2415–2439.
——, Z. Zhu, B. S. Giese, B. Huang, B. P. Kirtman, J. Shukla, and J. A. Carton, 1997: Annual cycle and ENSO in a coupled ocean–atmosphere general circulation model. *Mon. Wea. Rev.,* **125,** 680–702.
Sela, J. M., 1980: Spectral modeling at the National Meteorological Center. *Mon. Wea. Rev.,* **108,** 1279–1292.
Singer, J. J., 1990: On the error observed in electronically digitized T-7 XBT data. *J. Atmos. Oceanic Technol.,* **7,** 603–611.
Slingo, J. M., 1987: The development and verification of a cloud prediction scheme for the ECMWF model. *Quart. J. Roy. Meteor. Soc.,* **113,** 899–927.
Stockdale, T. N., 1997: Coupled ocean–atmosphere forecasts in the presence of climate drift. *Mon. Wea. Rev.,* **125,** 809–818.
——, D. L. T. Anderson, J. O. S. Alves, and M. A. Balmaseda, 1998: Global seasonal rainfall forecasts using a coupled ocean–atmosphere model. *Nature,* **392,** 370–373.
Suarez, M. J., and P. S. Schopf, 1988: A delayed action oscillator for ENSO. *J. Atmos. Sci.,* **45,** 3283–3287.
Trenberth, K. E., W. G. Large, and J. G. Olson, 1990: The mean annual cycle in global ocean wind stress. *J. Phys. Oceanogr.,* **20,** 1742–1760.
Wright, D., and M. Szabados, 1989: Field evaluation of real-time XBT systems. *Oceans 89 Proc.,* **5,** 1621–1626.
Xue, Y., M. J. Fennessy, and P. J. Sellers, 1996: Impact of vegetation properties on U.S. summer weather prediction. *J. Geophys. Res.,* **101** (D3), 7419–7430.
Zhu, Z., and E. K. Schneider, 1995: Experimental multi-season ENSO predictions with an anomaly coupled general circulation model. COLA Rep. 10, 28 pp. [Available from COLA, 4041 Powder Mill Rd., Suite 302, Calverton, MD 20705.]